iScience

CellPress
OPEN ACCESS

Article

Reversible adhesion by type IV pili leads to formation of permanent localized clusters

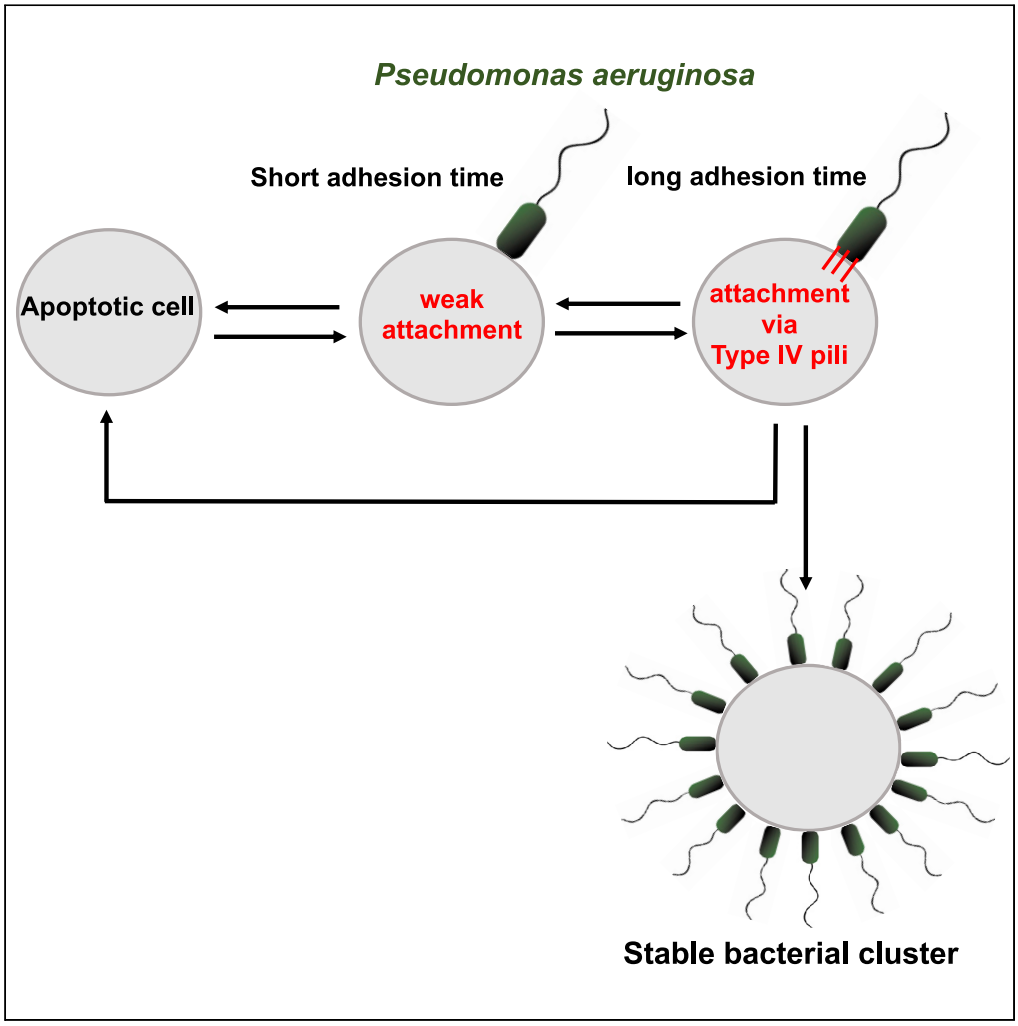

María Victoria Pepe, Celeste Dea, Camila Genskowsky, ..., Adriana Valeria Jäger, Fernando Peruani, Arlinet Kierbel

fernando.peruani@cyu.fr (F.P.)
akierbel@iibintech.com.ar (A.K.)

Highlights

P. aeruginosa adheres to apoptotic cells through a functional type-four pili

P. aeruginosa preferentially adheres to vesiculated apoptotic membranes

The formation of stable bacterial clusters does not require irreversible adhesion

Pepe et al., iScience 25, 105532
December 22, 2022
https://doi.org/10.1016/j.isci.2022.105532

iScience

CellPress
OPEN ACCESS

Article

Reversible adhesion by type IV pili leads to formation of permanent localized clusters

María Victoria Pepe,[1,3] Celeste Dea,[1,3] Camila Genskowsky,[1] Darío Capasso,[1] Mara Sabrina Roset,[1] Adriana Valeria Jäger,[1] Fernando Peruani,[2,*] and Arlinet Kierbel[1,4,*]

SUMMARY

The formation of long-lived, multicellular clusters is a fundamental step in the physiopathology of many disease-causing bacteria. Experiments on abiotic surfaces suggest that bacterial colonization, including initial cluster formation, requires (1) irreversible adhesion, (2) cell proliferation, and (3) a phenotypic transition. However, here we show that on infection of a polarized MDCK epithelium, *Pseudomonas aeruginosa* (PA) forms long-lived – i.e., *permanent* – bacterial clusters without requiring irreversible adhesion, cell proliferation, or a phenotypic transition. By combining experiments and a mathematical model, we reveal that the cluster formation process is mediated by type IV pili (T4P). Furthermore, we unveil how T4P quantitatively operate during adhesion, finding that it is a stochastic process that involves an activation time, requires the retraction of pili, and results in reversible attachment. We explain how such reversible attachment process leads to the formation of permanent bacterial clusters and quantify the cluster growth dynamics.

The early stages of many infection processes, which remain poorly understood, require bacteria to localize suitable host tissues where to anchor and form bacterial multicellular structures such as biofilms.[1] Often, the tissue colonization starts with the formation of localized bacterial clusters.[2–6] Once within mature multicellular structures and biofilms, bacteria are embedded in the extracellular matrix, which can be self-produced and/or formed with material acquired from the host tissue,[7] and exhibit resistance to flows and importantly, an increased tolerance to antibiotics and immune system responses.

For technical reasons, as well as for its relevance in industrial applications, bacterial colonization and biofilm formation have been investigated mainly on abiotic (and generally spatially homogeneous) surfaces.[8–14] It has been observed that an initial population of planktonic bacteria undergoes various phases before actual colonization of the (abiotic) surface.[9,10,12] In the initial phase that elapses for several hours, the overwhelming majority of bacteria remains swimming in the fluid, and attach only reversibly to the surface.[8–10,12] During this phase, it is believed that the bacterial population, over repeated cycles of surface sensing and detachment, becomes progressively adapted for irreversible surface attachment.[11,12] This is evidenced in the next phase of the process by a sudden exponential growth of the surface bacterial population that leads to a quick surface coverage that involves irreversible attachment, bacterial proliferation, and extracellular matrix production.[8,12] For *Pseudomonas aeruginosa* (PA) on abiotic surfaces,[12,15,16] the initial reversible-attachment phase elapses for 20 h. It is only after this initial period that irreversible attachment leads to the formation of nascent bacterial clusters.[15]

The colonization of biotic surfaces, on the other hand, remains largely unexplored. Infection experiments with polarized MDCK cells have revealed that PA is able to form bacterial clusters primarily on apoptotic cells shedding from the epithelium whereas the rest of the monolayer seems resistant to PA adhesion.[17,18] It is well known that PA causes long-term infections in the lungs of cystic fibrosis patients and in chronic wounds,[2,19] where it can form antibiotic-resistant biofilms. Importantly, in these contexts, there are exacerbated numbers of apoptotic cells.[20] PA clusters that form on MDCK monolayers reach their final size in minutes and remain stable for hours.[17,18] How PA form such permanent clusters has not yet been known. Here, we investigate the growth dynamics of these PA clusters and the statistics of the bacterial adhesion times. By combining experiments and a mathematical model, we find that the cluster formation process is

[1]Instituto de Investigaciones Biotecnológicas, Universidad Nacional de San Martín (UNSAM), CONICET, Buenos Aires B1650HMP, Argentina

[2]Laboratoire de Physique Théorique et Modélisation, UMR 8089, CY Cergy Paris Université, 95302 Cergy-Pontoise, France

[3]These authors contributed equally

[4]Lead contact

*Correspondence: fernando.peruani@cyu.fr (F.P.), akierbel@iibintech.com.ar (A.K.)

https://doi.org/10.1016/j.isci.2022.105532

regulated by type IV pili (T4P), which are hair-like appendages that can be rapidly extended and retracted to generate active forces to move or adhere.[21,22] Furthermore, we reveal how T4P quantitatively operate during adhesion on the apoptotic cells, finding that it is a stochastic process that involves an activation time, requires the retraction of pili, and results in reversible adhesion. In addition, we quantify the cluster growth dynamics and explain how such reversible adhesion process leads to the formation of permanent bacterial clusters that are arguably the precursors of a full-scale tissue infection. In short, our study shows that long-lived bacterial cluster formation in PA on biotic surfaces does not require irreversible adhesion, cell proliferation, or a phenotypic transition, in sharp contrast to what has been reported for PA on abiotic surfaces.

RESULTS

Features of formed bacterial clusters

On the polarized MDCK epithelium, PA forms bacterial clusters, on sites of apical extrusion of apoptotic cells, which we refer to as clusters or aggregates. In the span of minutes, free-swimming bacteria are recruited on the surface of those apoptotic cells.[17,18] Round-shaped bacterial aggregates of approximately 10 microns diameter are observed after infecting MDCK monolayers with PA strain K for 1 h (Figures 1A and 1B).

We investigate how PA attaches to apoptotic cells, by measuring the angle between the longitudinal axis of the bacterium and the tangent of the cell surface; see Figure 1C, where only bacteria on the focal plane are taken into consideration. We find that bacteria attach to the host cell with the cell body parallel to the normal vector of the cell membrane. Note that this spatial arrangement allows bacteria to densely cover the host cell. In previous studies, interaction with a surface via the cell pole has been associated with a reversible attachment, whereas irreversible attachment has been thought to require the cell to orient parallel to the surface.[23] We recall that WT PA harbors one flagellum and a reduced number of T4P, located at the bacterium poles. To visualize the flagellated pole in live bacteria the monolayers are infected with PA expressing chemotaxis protein CheA bound to GFP (CheA-GFP). CheA has a unipolar localization pattern at the flagellated pole.[24–26] We find 74% of the bacteria attached to apoptotic cells by the pole opposite to CheA (Figure 1D) and therefore opposite to the flagellum, indicating that there is a preferential orientation and discouraging the idea that the flagellum plays a role of an adhesin in this system. Nonetheless, flagella are essential for aggregate formation. The aflagellated mutant Δ*fliC* (the gene *fliC* encodes the major component of the flagellum) is unable to form aggregates (Figure S1). This is expected as bacteria reach apoptotic cells by swimming.

Biotic surfaces can display complex and heterogeneous topographies. Particularly, the plasmatic membrane of apoptotic cells suffers dramatic changes as the apoptotic process evolves. Upon infection, most extruded apoptotic cells are fully covered with bacteria. However, in some apoptotic cells it is observed that bacteria are distributed heterogeneously over the membrane, with patches that are covered with bacteria and other areas that are bacteria-free. We investigate whether there are detectable differences between membrane areas occupied and unoccupied by bacteria. Notably, in areas where bacteria attach, AnnexinV labeling is more intense (Figure 1E and Video S1). The quantification indicates that there exists a positive correlation between fluorescence intensity and bacterial number (Spearman Correlation's coefficient $r = 0.77$, $p < 0.05$). Staining with a general membrane marker displays a similar result (Figure S2), suggesting that bacterial attachment occurs in zones of increased membrane surface availability. Then, infected and uninfected samples are analyzed by Scanning Electron Microscopy. Figure 1F shows an extruded apoptotic cell with heterogeneous areas of adhered bacteria. Notably, the surfaces covered with bacteria are filled with membrane-enclosed microvesicles or small apoptotic bodies. In contrast, the bacteria-free membrane is smooth. Importantly, extruded cells of vesiculated morphology were also present in uninfected samples. And PA adheres all over the surface of apoptotic cells that are fully covered by microvesicles. This kind of cell surface has an irregular topography (Figure S3). In recent years, surface roughness and topography have been found to be critical to bacterial adhesion.[13,14]Taken together, our results indicate that PA attaches to extruded apoptotic cells vertically, by the pole opposite the flagellum, and demonstrate preference for cell surfaces with an irregular topography.

Temporal dynamics of aggregate formation

Immediately after wild-type (WT) PA is released, apoptotic cells start to be visited by bacteria and aggregate formation begins. We quantify the growth of the cluster by counting the number of bacteria in three

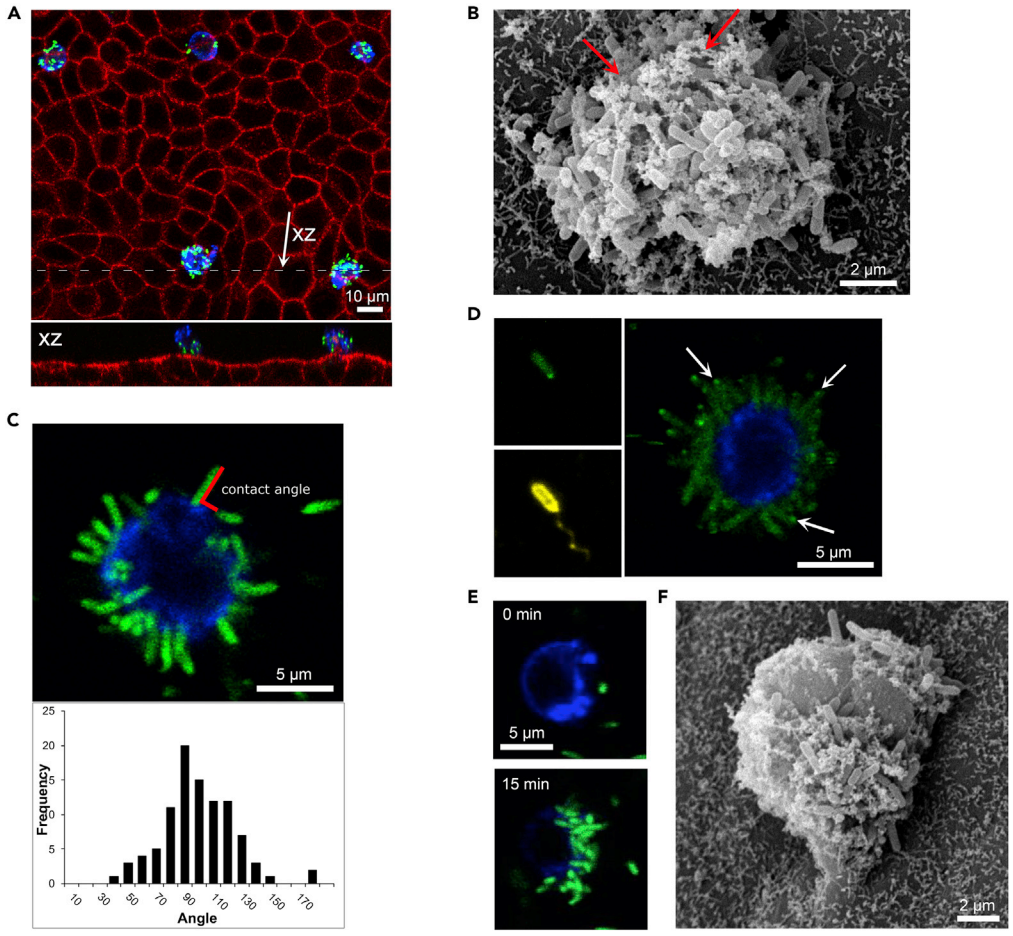

Figure 1. Morphology of formed PA aggregates

(A, B and F) Transwell grown MDCK monolayers were infected with PA, incubated for 1 h and fixed. (A) Top view and orthogonal section (upper and lower panel respectively) showing a confocal micrograph of a monolayer with several extruded apoptotic cells with adhered bacteria. After infection with PA-GFP (green), samples were labeled with Annexin V-Alexa 647 (blue), fixed, permeabilized and stained with phalloidin-rhodamine for F-actin (red). (B and F) Scanning electron micrographs. (B) Bacterial aggregate. Arrows indicate apoptotic host cell material.

(C–E) Time-lapse confocal microscopy images.Annexin V: blue. (C) The monolayer was infected with PA-GFP (green). Upper panel: Equatorial plane of an apoptotic cell. The angle between the longitudinal axis of bacteria and the tangent of the cell surface was measured as indicated. The 93% of the angles fell between 45 and 135° (lower panel) showing that bacteria attach by the pole. (D) CheA was used as a reporter of the flagellar pole (left panels show a fixed bacterium expressing CheA-GFP (green) and stained with an anti-PA antibody that labels the flagellum (yellow)). Right panel: time-lapse image of the equatorial plane of an apoptotic cell 15 min after infection. Bacteria attach by the pole opposite the flagellum. (E) Micrographs show the equatorial plane of the same apoptotic cell at the beginning (upper panel) and 15 min after infection (lower panel) with PA-GFP (green). Bacteria adhered to zones of more intense annexin V labeling.

(F) Bacteria attach to zones of the surface with vesiculated morphology.

dimensions as well as at the equatorial plane of the apoptotic cell as shown in Figures 2A, 2C and Video S2. Although both methods provide comparable information on the cluster dynamics, see Figures 2B and 2D, the latter allows a faster acquisition rate. Once clusters are formed, they remain stable in size for at least 3 h. The observed dynamics leads to the formation of stable bacterial clusters, in the sense that once formed, the cluster size remains roughly constant overtime, and thus the cluster is long-lived. However, careful inspection of the data shows that during cluster growth bacteria forming the cluster often detach and swim away from it, leaving an area of the apoptotic cell membrane vacant. This vacant membrane area is exposed to free-swimming bacteria, and thus at some later time becomes occupied again. The bacterial attachment-detachment process continues even in fully formed clusters. The reversible character of the adhesion process can be experimentally evidenced using two differentially labeled populations of PA, as shown in

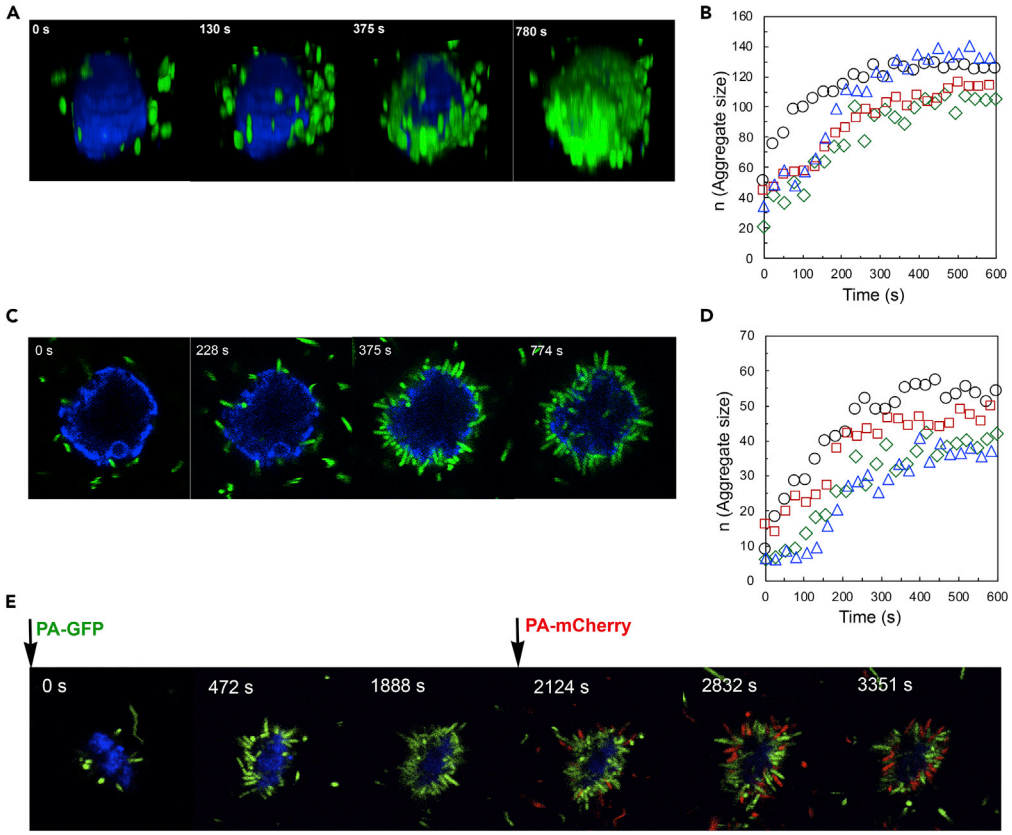

Figure 2. Formation of aggregates on apoptotic cells extruded from a monolayer

(A,C and E) Time-lapse confocal imaging of PA-GFP (green) adhering on apoptotic cells (blue). (A) 3D reconstructions of successive z-stacks (C) Snapshots of the equatorial plane of the cell.

(B and D) Growth curves of four different experimental aggregates. (B) The number of bacteria (aggregate size, denoted by *n*) was obtained from the entire z stack. (D) The number of bacteria found on the equatorial plane. (E) Snapshots of the equatorial plane in an experiment where initially the monolayer was inoculated with PA-GFP (green) and after 30 min PA-mCherry (red) was added.

Figure 2E and Video S3. Note that the reversible adhesion implies that clusters are dynamic structures. How can we characterize the observed growth dynamics and understand the emergence of long-lived, dynamical structures, when bacteria reversibly attach and detach from it? In order to quantify the cluster formation process, we focus on the dynamics of a small membrane area of the apoptotic cell that can be either vacant or occupied at most by a bacterium. Our first task is to characterize from the experiments the times during which the small membrane area is occupied; for details on the computation of these times see STAR Methods. The distribution of these times is presented in Figure 3A in the form of a survival curve $S(t)$, which indicates the probability of observing a dwelling time greater than or equal to t. Note that $S(t)$ for WT-PA in Figure 3A is not given by a simple exponential. Thus, if we attempt to mathematically model the dynamics assuming two states for the small membrane area – e.g., state 0 for vacant and state 1 for occupied, and transition rates r_{01} and r_{10} for transitions $0 \rightarrow 1$ and $1 \rightarrow 0$, respectively – we will fail to explain the experimentally obtained distribution $S(t)$. For a two-state Markov chain as described above, the survival curves associated with staying in state 0 and 1 are both, single exponential.

Mathematically, we can ensure the existence of (at least) three states: 0, 1, and 2, because a smaller number of states is not consistent with the measured distribution of dwelling times (see Figure 3A). Furthermore, states 1 and 2 necessarily correspond, both of them, to occupied states of the membrane area, whereas state 0 is the unoccupied state. But, what is the interpretation of states 1 and 2?.

To shed light on these two states, and on the role of T4P on the attachment process (i.e. the occupied states), we analyze experiments with T4P mutants: (1) Non-piliated Δ*pilA* mutant – PilA is the major pilin

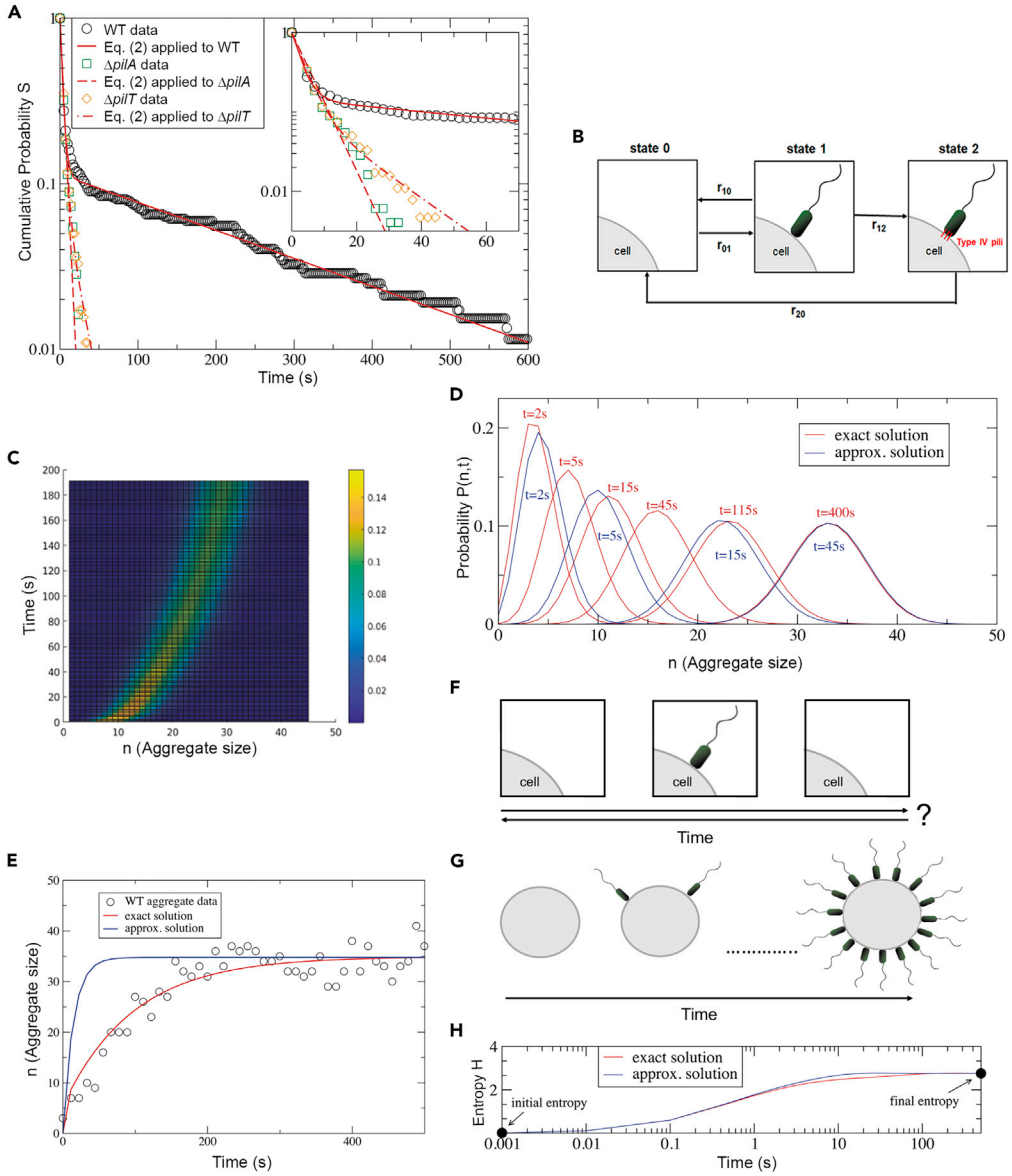

Figure 3. Growth dynamics of the aggregate

(A) Semi-log plot of the cumulative distribution of bacterial dwelling times on the cell membrane. Circles correspond to WT data, squares to Δ*pilA*data, and diamonds to the Δ*pilT* data, whereas the solid, dashed, and dotted-dashed curves to Equation2 applied to WT, Δ*pilA*, and Δ*pilT*data, respectively. The inset displays the distributions for short dwelling times, in the range $[0, 70]$.

(B) Scheme of the three-states model, see Equation1. For $r_{12} = 0$, the dynamics reduces to a 2-state model, with only states 0 and 1.

(C) Temporal evolution of the probability $P(n, t)$ (color coded) of finding that at time t the aggregate size is n; see Equation5.

(D) Comparison of the exact (red) and approximate (blue) solution of $P(n, t)$, evaluated at various times t.

(E) Aggregate size n versus time. Circles correspond to the growth of an experimental aggregate, while the red and blue curve correspond to exact and approximate solution of $P(n,t)$, respectively. Schemes (F) and (G) illustrates that the vacant-occupied dynamics of a small cell membrane area does not convey information about the arrow of time, (F), whereas from the temporal evolution of the aggregate is possible to identify it (G).

(H) The increase in entropy H, Equation6, puts in evidence the arrow of time and the irreversible character of the growth of the aggregate.

subunit – and ii) Hyperpiliated Δ*pilT* (– PilT is the molecular motor that mediates pilus retraction). Thus, deficient PilT strains are unable to retract their pili and thus, the characteristic retraction time associated with pili retraction should not be present in the dwelling time distribution. From the comparison between these mutants, we learn that a) clusters only emerge in WT (see Videos S4, S5, S6, and S7), b) two occupied states are required to account for dwelling-time distributions of WT and the *pilT* mutant, i.e., for bacteria displaying T4P, and c) the dwelling-time distribution is a single exponential for non-piliated Δ*pilA* only. Cluster formation was quantified in fixed samples. Neither Δ*pilA* nor Δ*pilT* or a *pilT* insertion mutant[27] (not shown) exhibit cluster formation on apoptotic cells (Figure S4). In consequence, state 2 is only present for bacteria equipped with T4P, i.e. WT and hyperpiliated, pili-retraction-deficient Δ*pilT*, and thus it can be associated with T4P-mediated adhesion. The dynamics among these states – see Figure 3B – is given by:

$$\partial_t p_0(t) = -r_{01}p_0 + r_{10}p_1 + r_{20}p_2, \quad \text{(Equation 1a)}$$

$$\partial_t p_1(t) = -(r_{12} + r_{10})p_1 + r_{01}p_0, \quad \text{(Equation 1b)}$$

$$\partial_t p_2(t) = -r_{20}p_2 + r_{12}p_1, \quad \text{(Equation 1c)}$$

where $p_i(t)$ is the probability of finding the small membrane area in state i and r_{ij} are the transition rates between state i and j.

Important clarification: initially, we considered in Equation1 all possible 6 transition rates, including r_{21} and r_{02}. However, the parameter selection (i.e. fitting) procedure (see below and STAR Methods) indicates that rates r_{21} and r_{02} are negligible and that a description based on only 4 rates, as displayed in Figure 3B, is mathematically preferable, because the same level of accuracy (i.e. goodness of the fit) is achieved with a reduced number of parameters. The absence of these two rates, as explained below, indicates that activation of T4P adhesion on the apoptotic cell is not instantaneous and involves a characteristic timescale (for WT-PA, presumably associated with pilus retraction). The rationale behind Equation1 and its rates is the following. The rate at which bacteria arrive to an unoccupied small membrane area is given by r_{01}. The rate at which a newly arrived (or weakly attached) bacterium swims away from the apoptotic cell is given by r_{10}. The rate r_{12} provides the rate at which the newly arrived or weakly attached bacterium transitions to a longer adhesion mode that below is shown to be related to T4P adhesion. Finally, r_{20} is the rate at which a bacterium in the long-adhesion mode detaches from the apoptotic cell. Thus, the temporal variation of the probability p_0 of finding a small cell membrane in state 0 (i.e., unoccupied) grows with transition $1 \rightarrow 0$ and $2 \rightarrow 0$ and decreases with $0 \rightarrow 1$, whereas p_1, the probability of being occupied by a weakly attached bacterium, increases by transition $1 \rightarrow 0$ and decreases $1 \rightarrow 2$ and $1 \rightarrow 0$. And the temporal variation of the probability p_2 of finding the small membrane area occupied by a bacterium in the long-adhesion mode increases with transitions $1 \rightarrow 2$ and decreases with $2 \rightarrow 0$.

From Equation 1, we compute $S(t)$ as a first-passage time problem that indicates for how long the system remains between state 1 and 2 before transitioning to 0, which reads:

$$S(t) = (1 - \varphi)e^{-(r_{10}+r_{12})t} + \varphi e^{-r_{20}t}, \quad \text{(Equation 2)}$$

where $\varphi = r_{12}/(r_{12} + r_{10} - r_{20})$. By applying Equation2 to describe the distributions in Figure 3A, we find $r_{10} = 0.28 \pm 0.01$ s^{-1}, $r_{12} = 0.03 \pm 0.01$ s^{-1}, and $r_{20} = 0.004 \pm 0.0009$ s^{-1} for WT, and $r_{10} = 0.25 \pm 0.01$ s^{-1}, $r_{12} = 0.02 \pm 0.01$ s^{-1}, and $r_{20} = 0.055 \pm 0.002$ s^{-1} for Δ*pilT* mutant; further details in STAR Methods. On the other hand, for Δ*pilA*data $r_{12} = 0$ and thus the model becomes effectively a two-state Markov chain, with only state 0 and 1 participating into the dynamics, and $S(t)$ reduces to $S(t) = e^{-r_{10}t}$, obtaining $r_{10} = 0.23 \pm 0.02$ s^{-1}. Note that the main difference between the rates of WT and Δ*pilT* is observed in r_{20} that is 10 times larger for the Δ*pilT*, which implies that dwelling times are expected to be in average one order of magnitude longer in WT. The similarity of the obtained values r_{10} in experiments with WT,Δ*pilT*, and Δ*pilA* mutants suggests that the transition $0 \rightarrow 1$ involves the same mechanism for WT and these mutants, which is evidently unrelated to T4P. In summary, the transition from $1 \rightarrow 2$ observed in WT and in Δ*pilT* indicates that adhesion mediated by T4P is a stochastic process that requires not only the presence of pili, but also the capability of retraction it to achieve long adhesion times. T4P are also involved in surface sensing, a process whereby surface engaged bacteria, through the Chp putative chemosensory system, upregulate synthesis of the second messenger cyclic AMP (cAMP) and initiate physiological changes required for surface-associated lifestyles.[28,29] PilH is one of the response regulators of the Chp

system that has been proposed to limit downstream signaling and/or to control the function of the retraction ATPase PilT.[28,30] Deletion of *pilH* results in high levels of cAMP and hyperpiliation. We found that Δ*pilH* clusters on apoptotic cells but to a lesser extent than the wt. To rule out the possibility that an alternative adhesin stimulated upon T4P-mediated surface sensing was involved in cluster formation, we also tested the Δ*pilH*Δ*pilB* double mutant. PilB is the molecular motor that mediates pili assembly. Thus, Δ*pilH*Δ*pilB* lacks surface pili but it would be constantly active for surface sensing. We found this mutant does not adhere to apoptotic cells for long adhesion times, and it is, therefore, unable to cluster, supporting the conclusion that the T4 pilus is the main adhesin in this system (see Videos S8, S9, and S10).

It is worth stressing that Equation 1 is the simplest 3-state Markov chain consistent with the experimental data: transition rates r_{02} and r_{21} can be also included in the description in order to allow all possible transitions, however, these extra two parameters do not improve the goodness of the fit; and thus including them leads to over-fitting. For further details on the derivation of Equation2 and fitting procedure, see STAR Methods. Now, we focus on the growth of the cluster. We consider the probability $P(n,t)$ of finding n bacteria on the apoptotic cell at time t, assuming the cell contains N statistically independent small membrane areas. Under these assumptions, we approximate the evolution of $P(n,t)$ by the following master equation:

$$\begin{aligned}\partial_t P(n,t) = & -[\Omega_+(n)+\Omega_-(n)]P(n,t) \\ & +\Omega_+(n-1)P(n-1,t)+\Omega_-(n+1)P(n+1,t),\end{aligned} \qquad \text{(Equation 3)}$$

where $\Omega_+(n)=\alpha_+(N-n)$ and $\Omega_-(n)=\alpha_- n$. The rate α_+ is directly $\alpha_+=r_{01}$ and describes how frequently swimming bacteria arrive at a vacant membrane area. Thus, this rate depends on bacterial motility as well as on bacterial density; the simplest assumption is that $\alpha_+ \propto C$, with C the inoculated bacterial concentration. On the other hand, α_- depends on intrinsic properties of the bacterium, i.e., on its adhesion capacity to the apoptotic cell membrane, and is given by inverse of the average time a bacterium remains on the cell membrane, related to $S(t)$ by:

$$[\alpha_-]^{-1} = \int_0^\infty dt' S(t') = \frac{1-\varphi}{r_{12}+r_{10}}+\frac{\varphi}{r_{20}}, \qquad \text{(Equation 4)}$$

implying, $\alpha_- = (r_{12}+r_{10})/\left[1+\frac{r_{12}}{r_{20}}\right]$. The solution of Equation 3 with the provided definitions of $\Omega_+(n)$ and $\Omega_-(n)$ and using as initial condition that at $t=0$ there is no bacteria on the cell – i.e. $P(n=0,t=0)=1$ and $P(n,t=0)=0$ for $n>0$ – reads:

$$P(n,t) = \binom{N}{n} q(t)^n (1-q(t))^{N-n} \qquad \text{(Equation 5)}$$

with $q(t)=\frac{\alpha_+}{\alpha_++\alpha_-}[1-e^{-(\alpha_++\alpha_-)t}]$; see Figures 3C and 3D. The binomial nature of Equation5 implies that $\langle n\rangle(t)=\sum_n n\ P(n,t)=q(t)N$. The advantage of the approximation given by Equation3 is that it allows us to show that the growth of the cluster can be conceived as a biased random walk in the cluster-size space: the walker can move from position n to either $n-1$ (after the detachment of a bacterium) or $n+1$ (if a bacterium attaches to the cell). The ratio of the transition probabilities $n\to n+1$ and $n\to n-1$ provides an idea of the local bias of the walker, which depends on n as well as on the ratio α_+/α_-; Figure 3D. At small values of n, the large availability of vacant sites, i.e. $N-n$, favors a bias toward large n-values, and the opposite happens for large values of n. If rates α_+ and α_- are identical, then the walkers move to, and remain around, $n_*=N/2$, but in general $\alpha_+/\alpha_-\neq 1$, and the equilibrium position corresponds to $n_*=N/(1+\alpha_-/\alpha_+)$. We note the critical dependency of α_- with r_{12}. In the limit of large r_{12} values, $\alpha_-\sim r_{20}$, whereas for $r_{12}\to 0$, $\alpha_-\to r_{10}$. Because $r_{20}\ll r_{10}$, the equilibrium position for WT, equipped with a fully functioning T4P, is expected to be much larger than the one for Δ*pilA* and Δ*pilT*. The analogy with the biased random walk allows us to conceptually understand the emergence of an irreversible dynamics for cluster growth out of the reversible, attachment-detachment action of individual bacteria. However, the approximated temporal evolution of $P(n,t)$ given by Equation3 assumes that transitions from $n\to n+1$, $n\to n-1$, etc are characterized by exponentially distributed times, which is certainly not true as evidenced by the distribution of dwelling times, Figure 3A. Nevertheless, it is possible to obtain an exact solution of the original problem using that at every time t the probability is given by the binomial distribution $P(n,t)=\binom{N}{n}\tilde{q}(t)^n(1-\tilde{q}(t))^{N-n}$, with $\tilde{q}(t)=p_1(t)+p_2(t)$, where $p_1(t)$ and $p_2(t)$ are the solutions of Equation1 with initial condition $p_0(t=0)=1$ and $p_1(t=0)=p_2(t=0)=0$; see STAR Methods for explicit expressions. In Figure 3E, the exact and approximate solution are used to describe temporal evolution of cluster size on an apoptotic

cell. The value of r_{01} is adjusted via the nonlinear least squares method obtaining $r_{01} = 0.037 \pm 0.002 s^{-1}$; for further details see STAR Methods. Note that the approximate solution fails to describe the temporal evolution toward the equilibrium cluster size, which indicates that considering three states is key to achieve a faithful quantification of the temporal dynamics; Figure 3E.

DISCUSSION

The dynamics of a small cell membrane area is such that it is at times vacant and at times occupied by a bacterium, undergoing a state cycle between vacant and occupied. This implies that if the dynamics of this small membrane area is recorded in a video, and is shown to us, we will not be able to determine whether it is played forwards or backwards, i.e., we will not be able to identify the arrow of time; see Figure 3F. On the other hand, if we watch a video of the evolution of the whole cluster, we can easily determine whether the video is played forward or backward, and thus the arrow of time (and irreversibility) becomes apparent; Figure 3G. The analogy with the biased random walk in cluster size space has allowed us to mathematically understand the emergence of irreversibility out of a reversible dynamics at the level of individual bacteria. A formal way to put in evidence the irreversible character of cluster growth is to define the (Shannon) entropy of this structure as:

$$H(t) = -\sum_{n=0}^{N} P(n,t) \quad \log[P(n,t)]. \qquad \text{(Equation 6)}$$

The temporal evolution of this quantity, which scales with the apoptotic cell size, is displayed in Figure 3H that shows that H starts at a low level and reaches a final larger entropy value as is expected in an irreversible process. As the system will not spontaneously (in average) decrease its entropy at a later time, the cluster will not disintegrate. Note that the behavior of $H(t)$ is almost identical for the exact and approximated solution of $P(n,t)$, implying that the cluster dynamic is irreversible for both. Mathematically, the approximated solution given by Equation3 is based on an effective reduction of the dynamics to two states, whereas the exact solution is based on three states. This indicates that mathematically the use of three states – which at microscopic level, according to Equation 1, involves entropy production – is not a necessary condition to obtain an irreversible cluster dynamics. Considering three states and their interplay is, however, essential, not for irreversibility, but to obtain an accurate description of dwelling times and of cluster growth, and unveils fundamental information on T4P-adhesion dynamics. In particular, state 2 is required for an accurate description of adhesion times of bacteria equipped with T4P. The presence of this state is a necessary, but not sufficient condition to observe long adhesion times and cluster formation (cf. WT, *pilT*, and Δ*pilA* mutants). In addition to the presence of T4P, pilus retraction is required for long-time adhesion (for membrane anchoring, cf. catch-bond adhesin dynamics[31]). Furthermore, the three-state model allows us to infer how T4P mediated adhesion works on the cell membrane: first, the bacterium needs to reach the cell membrane (transition $0 \rightarrow 1$), once in contact with the cell membrane in a weak adhesion mode, the bacterium requires an average of 33s (transition $1 \rightarrow 2$) to activate T4P-adhesion, and once activated, it keeps the bacterium attached to the membrane an average time of 4.3 min (transition $2 \rightarrow 0$), after which the bacterium detaches from the membrane and swims away. These findings are inline with recent results obtained by Koch et al.[32] that indicate that the T4P-apparatus operates by stochastically extending and retracting pili, and observe that these events are not triggered by surface contact. We note that the stochastic character of the adhesion process has also been evidenced in other bacterial systems, where interestingly, active adhesion has also been described by a two-step process,[33,34] an observation that suggests possible universal adhesion behaviors.

On the other hand, we recall that PA is temporally attached upright by the pole opposite to the flagellum; Figure 1D. It is worth mentioning that Schniederberend et al.[35] found that when the attachment is, contrary to what is reported here, mediated by the flagellum, irreversible adhesion is induced and PA ends up laying horizontally on the surface. This suggests that adhesion by the pole opposite to the flagellum is characteristic of transient adhesion mediated by T4P. We also observe that a few bacteria lay parallel to the cell surface. In the future, it would be interesting to explore whether attachment initiated by the flagellar pole (as we found in 26% of the cases) favors the acquisition of the horizontal position. Nonetheless, our mathematical model proves that the emergence of permanent clusters does not require an irreversible attachment state. We clarify that this does not exclude that at longer times that the ones investigated here, bacteria transition to irreversible attachment, but our study proves that it is not needed for the emergence of permanent clusters.

We note that PA-laden extruded cells may eventually detach from the epithelium. It can be speculated these clusters remain viable after coming off and keep evolving in suspension. In recent years, evidence has accumulated showing suspended-bacterial clusters, also called biofilm-like aggregates, is a major form of bacterial communities in chronic infections.[36] Such is the case of chronic PA infections in cystic fibrosis patients, where the suspended-bacterial clusters are embedded in host cell material.[3,5,6] Biofilm-like aggregates are much smaller (10–100 μm wide) than surface-attached biofilms and the mechanisms through which they are formed are yet not known. An alternative scenario is that clustered-PA may be killed by host cells. In,[18,37] it was shown that neighboring epithelial cells or macrophages can internalize PA-laden apoptotic cells through efferocytosis. Once inside the cell, PA is transported to lysosomes and eliminated.

Finally, we speculate on the functionality of the observed dynamical multicellular structures involving reversible attachment. An often invoked advantage of bacterial clustering is that it allows bacteria to cooperate by sharing "public goods". This can occur by collectively secreting enzymes into the surroundings in order to digest too large or insoluble materials.[38,39] As the amount of hydrolyzing enzymes increases, the local concentration of oligomers to uptake also does it.[40] Thus, it can be speculated that in clusters with a constant turnover of bacteria, the concentration of "public goods" (enzymes or signals) increases by allowing, overtime, a larger number of donors to participate.

Limitations of the study

The cluster formation dynamics was studied during 15 min, after which stable clusters were present in the system. We have verified that cluster sizes remain stable through approximately 3 h. However, we cannot exclude that bacteria modify their behavior after the studied initial 15-min period, despite the mathematical model proves that stable clusters can potentially emerge from reversible attachment. Longer experiments are required to settle the issue.

On the other hand, our model implies the presence of assembled pili localized at the pole of attachment on apoptotic cells. However, our study does not provide direct observation of pili localization. Direct visualization of pili is required to confirm this hypothesis.

STAR★METHODS

Detailed methods are provided in the online version of this paper and include the following:

- KEY RESOURCES TABLE
- RESOURCE AVAILABILITY
  - Lead contact
  - Materials availability
  - Data and code availability
- EXPERIMENTAL MODEL AND SUBJECT DETAILS
- METHODS DETAILS
  - Cell culture and bacterial infection
  - Time-lapse confocal microscopy
  - Immunofluorescence and scanning electron microcopy
  - Mathematical model and fitting procedure

SUPPLEMENTAL INFORMATION

Supplemental information can be found online at https://doi.org/10.1016/j.isci.2022.105532.

ACKNOWLEDGMENTS

We thank Joanne Engel and Yuki Inclan for PAK and PA01 mutant strains, Joseph P. Sheehan and Zemer Gitai for plasmid pJN(*cheA-gfp*) and Francisco Guaimas for technical assistance in microscopy imaging. Furthermore, we thank Pablo S. Aguilar and Alejandro Colman-Lerner for critical comments and suggestions. M.V.P, C.G and D.C, are research fellows at Consejo Nacional de Investigaciones Científicas y Técnicas (CONICET, Argentina). C.D is a research fellow at "Agencia Nacional de Promoción de la Investigación, el desarrollo teconológico y la innovación" (Agencia i + D + i). A.K., M.S.R and A.V.J are research career members of CONICET. F.P. acknowledges financial support from CY Initiative of Excellence (grant 'Investissements d'Avenir' ANR-16-IDEX-0008), INEX 2021 Ambition Project CollInt and Labex MME-DII,

projects 2021-258 and 2021-297. This work was supported by grants from Agencia i+D+i (PICT-I-D-2018, granted to A.V.J and PICT-2020-SERIEA-01669 granted to A.K.).

AUTHOR CONTRIBUTIONS

M.V.P., C.D., F.P., and A.K. designed research. M.V.P., C.D., C.G., D.C., F.P., and A.K. analyzed data. M.V.P., C.D., C.G., D.C., M.S.R., and A.V.J. performed research. F.P. and A.K. developed the mathematical model and wrote the paper.

DECLARATION OF INTERESTS

The authors declare no competing interests.

INCLUSION AND DIVERSITY

We support inclusive, diverse, and equitable conduct of research.

Received: February 2, 2022
Revised: May 25, 2022
Accepted: November 4, 2022
Published: December 22, 2022

REFERENCES

1. Otte, S., Ipiña, E.P., Pontier-Bres, R., Czerucka, D., and Peruani, F. (2021). Statistics of pathogenic bacteria in the search of host cells. Nat. Commun. *12*, 1990.

2. Bjarnsholt, T., Jensen, P.Ø., Fiandaca, M.J., Pedersen, J., Hansen, C.R., Andersen, C.B., Pressler, T., Givskov, M., and Høiby, N. (2009). Pseudomonas aeruginosa biofilms in the respiratory tract of cystic fibrosis patients. Pediatr.Pulmonol. *44*, 547–558.

3. Burmølle, M., Thomsen, T.R., Fazli, M., Dige, I., Christensen, L., Homøe, P., Tvede, M., Nyvad, B., Tolker-Nielsen, T., Givskov, M., et al. (2010). Biofilms in chronic infections–a matter of opportunity–monospecies biofilms in multispecies infections. FEMS Immunol. Med. Microbiol. *59*, 324–336.

4. Bjarnsholt, T., Alhede, M., Alhede, M., Eickhardt-Sørensen, S.R., Moser, C., Kühl, M., Jensen, P.Ø., and Høiby, N. (2013). The in vivo biofilm. Trends Microbiol. *21*, 466–474.

5. Sønderholm, M., Kragh, K.N., Koren, K., Jakobsen, T.H., Darch, S.E., Alhede, M., Jensen, P.Ø., Whiteley, M., Kühl, M., and Bjarnsholt, T. (2017). Pseudomonas aeruginosa aggregate formation in an alginate bead model system exhibits in vivo-like characteristics. Appl. Environ. Microbiol. *83*. e00113-17.

6. Jennings, L.K., Dreifus, J.E., Reichhardt, C., Storek, K.M., Secor, P.R., Wozniak, D.J., Hisert, K.B., and Parsek, M.R. (2021). Pseudomonas aeruginosa aggregates in cystic fibrosis sputum produce exopolysaccharides that likely impede current therapies. Cell Rep. *34*, 108782.

7. Karygianni, L., Ren, Z., Koo, H., and Thurnheer, T. (2020). Biofilm matrixome: extracellular components in structured microbial communities. Trends Microbiol. *28*, 668–681.

8. Wong, G.C.L., Antani, J.D., Lele, P.P., Chen, J., Nan, B., Kühn, M.J., Persat, A., Bru, J.L., Høyland-Kroghsbo, N.M., Siryaporn, A., et al. (2021). Roadmap on emerging concepts in the physical biology of bacterial biofilms: from surface sensing to community formation. Phys. Biol. *18*, 051501.

9. Armbruster, C.R., and Parsek, M.R. (2018). New insight into the early stages of biofilm formation. Proc. Natl. Acad. Sci. USA *115*, 4317–4319.

10. Berne, C., Ellison, C.K., Ducret, A., and Brun, Y.V. (2018). Bacterial adhesion at the single-cell level. Nat. Rev. Microbiol. *16*, 616–627.

11. Lee, C.K., de Anda, J., Baker, A.E., Bennett, R.R., Luo, Y., Lee, E.Y., Keefe, J.A., Helali, J.S., Ma, J., Zhao, K., et al. (2018). Multigenerational memory and adaptive adhesion in early bacterial biofilm communities. Proc. Natl. Acad. Sci. USA *115*, 4471–4476.

12. Lee, C.K., Vachier, J., de Anda, J., Zhao, K., Baker, A.E., Bennett, R.R., Armbruster, C.R., Lewis, K.A., Tarnopol, R.L., Lomba, C.J., et al. (2020). Social cooperativity of bacteria during reversible surface attachment in young biofilms: a quantitative comparison of pseudomonas aeruginosa pa14 and pao1. mBio *11*. e02644-19.

13. Wu, S., Zhang, B., Liu, Y., Suo, X., and Li, H. (2018). Influence of surface topography on bacterial adhesion: a review. Biointerphases *13*, 060801.

14. Song, F., Koo, H., and Ren, D. (2015). Effects of material properties on bacterial adhesion and biofilm formation. J. Dent. Res. *94*, 1027–1034.

15. Sauer, K., Camper, A.K., Ehrlich, G.D., Costerton, J.W., and Davies, D.G. (2002). Pseudomonas aeruginosa displays multiple phenotypes during development as a biofilm. J. Bacteriol. *184*, 1140–1154.

16. Davey, M.E., Caiazza, N.C., and O'Toole, G.A. (2003). Rhamnolipid surfactant production affects biofilm architecture in pseudomonas aeruginosa pao1. J. Bacteriol. *185*, 1027–1036.

17. Lepanto, P., Bryant, D.M., Rossello, J., Datta, A., Mostov, K.E., and Kierbel, A. (2011). Pseudomonas aeruginosa interacts with epithelial cells rapidly forming aggregates that are internalized by a lyn-dependent mechanism. Cell Microbiol. *13*, 1212–1222.

18. Capasso, D., Pepe, M.V., Rossello, J., Lepanto, P., Arias, P., Salzman, V., and Kierbel, A. (2016). Elimination of pseudomonas aeruginosa through efferocytosis upon binding to apoptotic cells. PLoS Pathog. *12*. e1006068.

19. Serra, R., Grande, R., Butrico, L., Rossi, A., Settimio, U.F., Caroleo, B., Amato, B., Gallelli, L., and de Franciscis, S. (2015). Chronic wound infections: the role of pseudomonas aeruginosa and staphylococcus aureus. Expert Rev. Anti Infect. Ther. *13*, 605–613.

20. Soleti, R., Porro, C., and Martínez, M.C. (2013). Apoptotic process in cystic fibrosis cells. Apoptosis *18*, 1029–1038.

21. Denise, R., Abby, S.S., and Rocha, E.P.C. (2019). Diversification of the type iv filament superfamily into machines for adhesion, protein secretion, dna uptake, and motility. PLoS Biol. *17*. e3000390.

22. Chang, Y.-W., Rettberg, L.A., Treuner-Lange, A., Iwasa, J., Søgaard-Andersen, L., and Jensen, G.J. (2016). Architecture of the type iva pilus machine. Science *351*, aad2001.

23. Caiazza, N.C., and O'Toole, G.A. (2004). Sadb is required for the transition from reversible to irreversible attachment during biofilm

formation by pseudomonas aeruginosa pa14. J. Bacteriol. *186*, 4476–4485.

24. Güvener, Z.T., Tifrea, D.F., and Harwood, C.S. (2006). Two different pseudomonas aeruginosa chemosensory signal transduction complexes localize to cell poles and form and remould in stationary phase. Mol. Microbiol. *61*, 106–118.

25. Murray, T.S., and Kazmierczak, B.I. (2006). Flhf is required for swimming and swarming in pseudomonas aeruginosa. J. Bacteriol. *188*, 6995–7004.

26. Cowles, K.N., Moser, T.S., Siryaporn, A., Nyakudarika, N., Dixon, W., Turner, J.J., and Gitai, Z. (2013). The putative poc complex controls two distinct p seudomonas aeruginosa polar motility mechanisms. Mol. Microbiol. *90*, 923–938.

27. Whitchurch, C.B., and Mattick, J.S. (1994). Characterization of a gene, pilu, required for twitching motility but not phage sensitivity in pseudomonas aeruginosa. Mol. Microbiol. *13*, 1079–1091.

28. Bertrand, J.J., West, J.T., and Engel, J.N. (2010). Genetic analysis of the regulation of type iv pilus function by the chp chemosensory system of pseudomonas aeruginosa. J. Bacteriol. *192*, 994–1010.

29. Whitchurch, C.B., Leech, A.J., Young, M.D., Kennedy, D., Sargent, J.L., Bertrand, J.J., Semmler, A.B.T., Mellick, A.S., Martin, P.R., Alm, R.A., et al. (2004). Characterization of a complex chemosensory signal transduction system which controls twitching motility in pseudomonas aeruginosa. Mol. Microbiol. *52*, 873–893.

30. Silversmith, R.E., Wang, B., Fulcher, N.B., Wolfgang, M.C., and Bourret, R.B. (2016). Phosphoryl group flow within the pseudomonas aeruginosa pil-chp chemosensory system: differential function of the eight phosphotransferase and three receiver domains. J. Biol. Chem. *291*, 17677–17691.

31. Thomas, W.E., Vogel, V., and Sokurenko, E. (2008). Biophysics of catch bonds. Annu. Rev. Biophys. *37*, 399–416.

32. Koch, M.D., Fei, C., Wingreen, N.S., Shaevitz, J.W., and Gitai, Z. (2021). Competitive binding of independent extension and retraction motors explains the quantitative dynamics of type iv pili. Proc. Natl. Acad. Sci. USA *118*. e2014926118.

33. Perez Ipiña, E., Otte, S., Pontier-Bres, R., Czerucka, D., and Peruani, F. (2019). Bacteria display optimal transport near surfaces. Nat. Phys. *15*, 610–615.

34. Pierrat, X., Wong, J.P.H., Al-Mayyah, Z., and Persat, A. (2021). The mammalian membrane microenvironment regulates the sequential attachment of bacteria to host cells. mBio *12*. e0139221.

35. Schniederberend, M., Williams, J.F., Shine, E., Shen, C., Jain, R., Emonet, T., and Kazmierczak, B.I. (2019). Modulation of flagellar rotation in surface-attached bacteria: a pathway for rapid surface-sensing after flagellar attachment. PLoS Pathog. *15*. e1008149.

36. Cai, Y.-M. (2020). Non-surface attached bacterial aggregates: a ubiquitous third lifestyle. Front. Microbiol. *11*, 557035.

37. Jäger, A.V., Arias, P., Tribulatti, M.V., Brocco, M.A., Pepe, M.V., and Kierbel, A. (2021). The inflammatory response induced by pseudomonas aeruginosa in macrophages enhances apoptotic cell removal. Sci.Rep. *11*, 1–13.

38. Hehemann, J.-H., Arevalo, P., Datta, M.S., Yu, X., Corzett, C.H., Henschel, A., Preheim, S.P., Timberlake, S., Alm, E.J., and Polz, M.F. (2016). Adaptive radiation by waves of gene transfer leads to fine-scale resource partitioning in marine microbes. Nat. Commun. *7*, 12860.

39. Wargacki, A.J., Leonard, E., Win, M.N., Regitsky, D.D., Santos, C.N.S., Kim, P.B., Cooper, S.R., Raisner, R.M., Herman, A., Sivitz, A.B., et al. (2012). An engineered microbial platform for direct biofuel production from brown macroalgae. Science *335*, 308–313.

40. Ratzke, C., and Gore, J. (2016). Self-organized patchiness facilitates survival in a cooperatively growing bacillus subtilis population. Nat. Microbiol. *1*, 16022.

STAR★METHODS

KEY RESOURCES TABLE

REAGENT or RESOURCE	SOURCE	IDENTIFIER
Antibodies		
Anti-*P. aeruginosa*	Abcam	Cat# ab68538; RRID: AB_1270071
Bacterial and virus strains		
P. aeruginosa K (PAK) WT	Stephen Lory's Laboratory	Figures 1–3. Videos S1, S2, S3, S4, and S6
P. aeruginosa K (PAK) Δ*fliC*	Stephen Lory's Laboratory	Figure S1
P. aeruginosa K (PAK) Δ*pilA*	Joanne Engel's Laboratory	Figures 3A and S4A; Videos S4 and S5
P. aeruginosa K (PAK) Δ*pilT*	Joanne Engel's Laboratory	Figures 3A and S4B and Videos S6 and S7
P. aeruginosa K (PAK) Ω*pilT* (*pilT* insertion mutant), tetracycline-resistant	John Mattick's Laboratory	N/A
P. aeruginosa 01 (PA01) WT	John Mattick's Laboratory	Video S8
P. aeruginosa 01 (PA01) Δ*pilH*	Joanne Engel's Laboratory	Video S9 (26)
P. aeruginosa 01 (PA01) Δ*pilH* Δ*pilB*	Joanne Engel's Laboratory	Video S10 (26)
Chemicals, peptides, and recombinant proteins		
Alexa Fluor 647 conjugated Annexin V	Thermo Fisher Scientific	Cat#: A23204
Rhodamine-Phalloidin	Thermo Fisher Scientific	Cat#: R415
CellMask Deep Red	Thermo Fisher Scientific	Cat#: C10046
Experimental models: Cell lines		
MDCK cells (Madin Darby Canine Kidney Cell Line, clone II)	Keith Mostov's Laboratory	N/A
Oligonucleotides		
Primer PilA-EcoRI-F CTCAAGAATTCATGAAAGCTCAAAAAGGC	This paper	N/A
Primer pilA-HindIII-R TCAAGCTTTTACTTAGAGCAACCTTTCGG	This paper	N/A
Primer PilT-BamHI-F CGGGATCCATGGATATTACCGAGCTGC	This paper	N/A
Primer PilT-HindII-R CCCAAGCTTCAGGATCAGAAGTTTTCCG	This paper	N/A
Recombinant DNA		
pJN-*cheA-gfp*	*Mol. Micro*, 90, 923–938, 2013	N/A
pMP7605-mCherry	FEMS Microbiol Lett. 2010; 305(1):81–90	N/A
pBBR1MCS-5 + *gfpmut3*	This paper	N/A
pSV35 + *pilA* (Carries a WT copy of *pilA*, for complementation of the Δ*pilA* strain). IPTG inducible	This paper	N/A
pSV35 + *pilT* (Carries a WT copy of *pilT*, for complementation of the Δ*pilT* strain). IPTG inducible	This paper	N/A
Software and algorithms		
ImageJ software	National Institutes of Health, NIH, USA	https://imagej.nih.gov/ij
Statistical methods and simulation used customized scripts implemented in MATLAB.	Impl This paper	
GraphPad Prism version 6.00 for Windows	GraphPad Software, La Jolla CaliforniaUSA	www.graphpad.com
Other		
glass-bottom dishes with a 35 mm micro-well	MatTek Corporation	P35G-1.5-14-C
12-mm transwells	Corning	3401

RESOURCE AVAILABILITY

Lead contact

Further information and requests for resources and reagents should be directed to and will be fulfilled by the lead contact, Dr. Arlinet Kierbel (akierbel@iibintech.com.ar).

Materials availability

Plasmids generated in this study are available from the lead contact upon request.

Data and code availability

- Adhesion time data are available from the lead contact upon reasonable request.
- Computer codes used to analyze and simulate the data are available from Dr. Fernando Peruani (fernando.peruani@cyu.fr) upon reasonable request.
- Further details on the model and fitting procedure are available from Dr. Fernando Peruani upon reasonable request.

EXPERIMENTAL MODEL AND SUBJECT DETAILS

Bacterial strains used in this work are listed in the key resources table. Bacteria were routinely grown shaking overnight in Luria-Bertani broth at 37 °C with appropriate antibiotic when required.

METHODS DETAILS

Cell culture and bacterial infection

MDCK cells (clone II, generously gifted by Dr. Keith Mostov) were cultured in MEM containing 5 % fetal bovine serum. For time-lapse experiments cells were grown on glass-bottom dishes with a 35 mm micro-well (MatTek Corporation). Around 10^4 cells per cm^2 were seeded and then kept for 72 h in culture to ensure the formation of fully polarized monolayers. For studies with fixed samples, cells were grown on 12 mm transwells (Corning Fisher, 4.5×10^5 cells per transwell) and used for experiments after 48 h in culture. Annexin V-Alexa-647 staining was done in binding buffer (10 mM HEPES, 140 mM NaCl and 2.5 mM CaCl2, pH 7.4). Stationary-phase bacteria were co-incubated with epithelial cells at a MOI of 20 for confocal studies, and at a MOI of 60, for scanning electron microscopy studies. *P. aeruginosa* K (PAK) strains WT and Δ*fliC*, Δ*pilA* and *pilT* mutants (kindly provided by J. Engel) were used. For CheA localization experiments the plasmid pJN(*cheA-gfp*) was used.[26]

Time-lapse confocal microscopy

Monolayers were washed with binding buffer, incubated with Alexa conjugated-Annexin V for 15 min (Annexin V binds to phosphatidylserine, which is located on the outer leaflet of the apopototic cell membrane) and then washed with MEM. Monolayers were then incubated in MEM supplemented with HEPES 20 mM. Micro-well dishes were placed on the microscope stage and the stack dimensions were set up from top to bottom throughout one or a few apoptotic cells (10 confocal optical sections at 1 μm intervals). Fluorescent bacteria were inoculated and immediately after image acquisition was started. This process was conducted at 25 °C. Alternatively, only the equatorial plane of the cell was scanned. Images were recorded with a confocal laser-scanning microscope Olympus FV1000, using a PlanApo N (60×1.42 NA) oil objective. The image size was 512×512 pixels. To measure "residence times" monolayers were inoculated with a mix of *P. aeruginosa*-GFP and *P-aeruginosa*-mCherry (1:3, final MOI = 20). In these experiments images were acquired at 2.33 s/frame. To track green bacteria and establish the attachment and detachment times, we used the MTrackJ plugin from the ImageJ software (National Institutes of Health, NIH, USA). MTrackJ plugin facilitates manual tracking of moving objects in image sequences.

Immunofluorescence and scanning electron microcopy

Bacteria carrying the CheA-GFP plasmid were allowed to adhere to polylysine-treated slides for 30 min at room temperature. Samples were fixed with 4 % paraformaldehyde in PBS for 15 min, blocked with BSA 1 % , and incubated overnight at 4 °C with the Anti- *P. aeruginosa* antibody. To measure the number of bacteria per aggregate, transwell-grown MDCK-monolayers were infected with the indicated strains for 1 h (MOI: 20). Samples were labeled with Alexa conjugated-Annexin V, fixed, blocked, permeabilized with saponin 0.1 %, stained with Alexa fluor-conjugated phalloidin for 60 min, and analyzed by confocal

microscopy. The image size was 1024 × 1024, and the z stack interval 0.3 μm. For scanning electron microscopy, transwell-grown MDCK monolayers were infected with *P. aeruginosa* for 1 h. Samples were washed with 0.15M Sorensen buffer (0.056 M NaH2PO4, 0.144 M Na2HPO4 pH = 7.2) and fixed with 2.5 % glutaraldehyde in 0.1M Sorensen buffer for 1hat room temperature. Samples were then washed, and progressive dehydration was carried out. After critical point drying and gold sputtering, samples were analyzed with a Carl Zeiss NTS Supra 40 microscope.

Mathematical model and fitting procedure

We provide details on the exact solution of Equation 1, the derivation of $S(t)$, and the fitting procedure.

Exact solution of Equation1.– Let us first recast Equation1 as:

$$\partial_t \mathbf{p} = M\mathbf{p},$$

where $\mathbf{p} = (p_0, p_1, p_2)^T$ and

$$M = \begin{pmatrix} -r_{01} & r_{10} & r_{20} \\ r_{01} & -(r_{12}+r_{10}) & 0 \\ 0 & r_{121} & -r_{20} \end{pmatrix}.$$

We use as initial condition: $\mathbf{p}(t=0) = (1,0,0)^T$. The exact solution takes the form $\mathbf{p} = c_0 \exp(\lambda_0 t)\mathbf{V}_0 + c_1 \exp(\lambda_1 t)\mathbf{V}_1 + c_2 \exp(\lambda_2 t)\mathbf{V}_2$. The eigenvalues are $\lambda_0 = 0$, $\lambda_1 = (-\omega - \beta)/2$, $\lambda_2 = (-\omega + \beta)/2$, with $\omega = r_{01} + r_{10} + r_{12} + r_{20}$, $\beta = \sqrt{\omega^2 - 4\gamma}$, where $\gamma = r_{01}(r_{12} + r_{20}) + r_{20}(r_{10} + r_{12})$, their corresponding eigenvectors are:

$$\mathbf{v}_0 = \left(\frac{r_{20}(r_{10}+r_{12})}{r_{01}r_{12}}, \frac{r_{20}}{r_{12}}, 1\right)^T$$

$$\mathbf{v}_1 = \left(-\frac{u_1 - \beta}{2r_{12}}, -\frac{u_2 + \beta}{2r_{12}}, 1\right)^T$$

$$\mathbf{v}_2 = \left(-\frac{u_1 + \beta}{2r_{12}}, -\frac{u_2 - \beta}{2r_{12}}, 1\right)^T,$$

where $u_1 = -r_{01} - r_{10} + r_{12} + r_{20}$ and $u_2 = r_{01} + r_{10} + r_{12} - r_{20}$. Finally, the coefficients are $c_0 = \frac{r_{01}r_{12}}{\gamma}$, $c_1 = \frac{r_{01}r_{12}(\omega-\beta)}{2\gamma\omega}$, and $c_2 = -\frac{r_{01}r_{12}(\omega+\beta)}{2\gamma\omega}$. We stress that $\tilde{q}(t) = p_1(t) + p_2(t)$, used to construct the exact solution $P(n,t)$ in the main text, corresponds to this solution, and should not be confused with $S(t)$.

Derivation of $S(t)$

From Equation1, $S(t)$ is computed as a first-passage problem: assuming that at $t = 0$ the state is 1, we estimate for how long state remains between 1 and 2, before transitioning back to 0. The system to solve is:

$$\partial_t p_1(t) = -(r_{12} + r_{10})p_1, \qquad \text{(Equation 8a)}$$

$$\partial_t p_2(t) = -r_{20}p_2 + r_{12}p_1, \qquad \text{(Equation 8b)}$$

with initial condition $p_1(t=0) = 1$ and $p_2(t=0) = 0$. The survival probability $S(t)$ is directly $S(t) = p_1(t) + p_2(t)$, whose explicit solution is given by Equation2. It is important to stress that $S(t)$ is not $p_1(t) + p_2(t)$ of Equation1, but of Equation8 with the specified initial conditions.

Fitting procedure

For the analysis of the dwelling times, we have to consider that we are limited by the duration of the experiment. In consequence, there are dwelling events, where we observe the beginning, i.e. when the bacterium attaches to the membrane, but not the end of the event, i.e. when the bacterium detaches, since we arrive at the end of the experiment. We classify dwelling times in two categories: those where we have observed the beginning and the end of the event (uncensored data), and those where we have observed the beginning, but not the end, which we analyzed using the Kaplan-Meier method. The fitting of data is obtained by applying nonlinear least squares to the obtained analytical expressions. We find using Equation2 for uncensored data, $r_{10} = 0.28\text{s}^{-1}$, $r_{12} = 0.03\text{s}^{-1}$, and $r_{20} = 0.004\text{s}^{-1}$ [$\chi^2 = 0.007$, $R^2 = 0.997$], while for the Kaplan-Meier method, $r_{10} = 0.29\text{s}^{-1}$, $r_{12} = 0.09\text{s}^{-1}$, and $r_{20} = 0.002\text{s}^{-1}$ [$\chi^2 = 0.01$,

R^2 = 0.98]; (Figure S5). In Δ*pilA*data, r_{12} = 0 and r_{10} = 0.23s^{-1} [χ^2 = 0.004, R^2 = 0.998], and in Δ*pilT*data, r_{10} = 0.25 s^{-1}, r_{12} = 0.02 s^{-1}, and r_{20} = 0.055 s^{-1} [χ^2 = 0.001, R^2 = 0.999]. censoringdata for Δ*pilA* and Δ*pilT* mutants is not necessary given the short duration of dwelling times. Finally, the description of aggregate growth is performed via $P(n,t)$. All parameters, but r_{01} are determined by the dwelling time distribution. Using the set of rates corresponding to the uncensored data, we find r_{01} = 0.04s^{-1} [χ^2 = 3075.7, R^2 = 0.90], and with the ones for all data, r_{01} = 0.035s^{-1} [χ^2 = 3535.3, R^2 = 0.88]; (Figure S5).